Front. Phys. 13(2), 137104 (2018)
https://doi.org/10.1007/s11467-017-0741-3

RESEARCH ARTICLE

Exotic ferromagnetism in the two-dimensional quantum material C_3N

Wen-Cheng Huang[1,2], **Wei Li**[3,†], **Xiaosong Liu**[1,2,4,‡]

[1] *State Key Laboratory of Functional Materials for Informatics, Shanghai Institute of Microsystem and Information Technology, Chinese Academy of Sciences, Shanghai 200050, China*
[2] *CAS Center for Excellence in Superconducting Electronics, Shanghai 200050, China*
[3] *Department of Physics and State Key Laboratory of Surface Physics, Fudan University, Shanghai 200433, China*
[4] *School of Physical Science and Technology, ShanghaiTech University, Shanghai 201210, China*
Corresponding authors. E-mail: [†] *w_li@fudan.edu.cn,* [‡] *xliu3@mail.sim.ac.cn*
Received September 26, 2017; accepted November 21, 2017

The search for and study of exotic quantum states in novel low-dimensional quantum materials have triggered extensive research in recent years. Here, we systematically study the electronic and magnetic structures in the newly discovered two-dimensional quantum material C_3N within the framework of density functional theory. The calculations demonstrate that C_3N is an indirect-band semiconductor with an energy gap of 0.38 eV, which is in good agreement with experimental observations. Interestingly, we find van Hove singularities located at energies near the Fermi level, which is half that of graphene. Thus, the Fermi energy easily approaches that of the singularities, driving the system to ferromagnetism, under charge carrier injection, such as electric field gating or hydrogen doping. These findings not only demonstrate that the emergence of magnetism stems from the itinerant electron mechanism rather than the effects of local magnetic impurities, but also open a new avenue to designing field-effect transistor devices for possible realization of an insulator–ferromagnet transition by tuning an external electric field.

Keywords quantum material, ferromagnetism

PACS numbers 71.20.Nr, 73.20.At, 75.70.Ak

1 Introduction

As a result of the confinement of space dimensionality, low-dimensional quantum materials display many unusual physical phenomena, such as the integer and fractional quantum Hall effects observed in gallium arsenide heterostructures [1, 2] in the 1980s. In 2004, the massless linear Dirac fermion was first observed in the monolayer form of graphite, graphene [3]. The search for exotic two-dimensional quantum materials with novel physical properties has attracted considerable research attention from both the condensed matter physics and material science communities. During the past decade, there have been progressive studies focusing on non-graphene layered materials, including transition-metal dichalcogenides [4], black phosphorus [5], and stanene [6]. These quantum materials display various band structures and have potential applications in optoelectronic technology. In contrast, the gapless energy band structure of graphene makes it difficult to fabricate graphene-based semiconducting devices, which have poor on–off current ratios ($I_{ON}/I_{OFF} < 100$) [7] and slow behavior in real circuit applications [8, 9]. These limitations of graphene in practical applications have encouraged attempts to extend the graphene family to crystalline two-dimensional layered materials made of similar elements [10].

Theoretical calculations have suggested two stable ordered semiconducting nitrogen-doped graphene structures, C_3N and $C_{12}N$, through the cluster expansion technique and particle swarm optimization method [11]. C_3N has been synthesized experimentally by direct pyrolysis of hexaaminobenzene trihydrochloride single crystals in the solid state [12] and polymerization of 2, 3-diaminophenazine by one of the coauthors of this paper [13]. Importantly, the coauthor has even conducted electronic band structure calculations suggesting that ferro-

© Higher Education Press and Springer-Verlag GmbH Germany, part of Springer Nature 2018

magnetism can be induced in hydrogen-doped C_3N and then realized it experimentally [13]. However, this type of magnetic behavior seems to be ascribed to the itinerant electron mechanism rather than the effects of local magnetic impurities [14], so the physical mechanism remains unclear.

In this paper, we elucidate the nature of ferromagnetism in charge-doped C_3N in detail using density functional theory. First, we perform lattice structure optimization and phonon dispersion calculations for C_3N using various exchange-correlation functions and find that the generalized gradient approximation (GGA) is more suitable for simulating the electronic band structure of C_3N than the local-density approximation (LDA). The electronic band dispersion reveals an indirect-band semiconductor with an energy gap of 0.38 eV, in good agreement with experiments [12, 13]. Interestingly, we notice that the van Hove singularities are located at energies near the Fermi level, ± 1 eV, which is half that of graphene. Thus, it is easy to inject charge carriers into C_3N and move the Fermi level so that it approaches the singularities. As a result, the nonmagnetic state becomes unstable against ferromagnetism [14]. Furthermore, calculations of the momentum ($\boldsymbol{q}$)-dependent electron susceptibility $\chi_0(\boldsymbol{q})$ reveal a sharp peak at $\boldsymbol{q} = 0$, supporting this scenario. Finally, we also perform a magnetic calculation for hydrogen-doped C_3N and further confirm that the ground state of $C_3NH_{0.125}$ is ferromagnetic, with a moment per unit cell of 0.1 μ_B. These calculations demonstrate that the magnetism is described mainly by the itinerant electron theory rather than local magnetic impurity theories, such as RKKY theory [15]. More importantly, these calculations suggest a new approach to realizing an insulator–ferromagnet transition in C_3N by tuning an external electric field, which may have potential applications in the development of novel electronic field-effect transistor devices.

The rest of this paper is organized as follows. In Section 2, we present the detailed theoretical methods. The results of theoretical calculations are presented and discussed in Section 3. Finally, we give a brief conclusion in Section 4.

2 Theoretical methods

The first-principles calculations presented in this work were performed using the projector augmented wave technique as implemented in the VASP code [16]. Throughout the calculations, a 400 eV cutoff in the plane-wave expansion and a $9\times9\times1$ Gamma $\boldsymbol{k}$ grid were chosen to ensure that the calculations had an accuracy of 10^{-5} eV. Further, all the structures, including the lattice constants and their internal coordinates, were optimized until the forces on individual atoms were smaller than 10^{-5} eV/Å to obtain sufficient accuracy. To reduce the interaction between neighboring layers, a vacuum slab of 15 Å along the z axis was introduced. When we study the effects of hydrogen doping of C_3N, a $4\times6\times1$ supercell structure was used for the calculations. In addition, the phonon dispersion was calculated using the density functional perturbation theory within the phonopy code [17].

3 Theoretical results and discussions

The lattice structure of C_3N, as shown in Fig. 1(a), can be regarded as a 2×2 superstructure of ordered nitrogen-doped graphene, where the doped nitrogen atoms themselves form a honeycomb lattice, similar to that of graphene but with twice the lattice constant. Consequently, the carbon atoms are separated into isolated six-membered rings. The lattice constant of C_3N as well as its internal coordinates are optimized using the following exchange-correlation potentials: the LDA, the GGA as proposed by Perdew and Wang (PW91) [18], and the GGA as proposed by Perdew, Burke, and Ernzerhof (PBE) [19]. In Fig. 1(b), we show the total energy difference ΔE as a function of various lattice constants in relation to the equilibrium position under the different exchange-correlation potentials. The equilibrium lattice constants are determined by fitting by the Birch–Murnaghan equation [20, 21] and are 4.817, 4.861, and 4.859 Å for the LDA, PBE, and PW91, respectively.

Next, we examine the stability of the lattice structure of C_3N obtained using various exchange-correlation potentials. The corresponding phonon spectra are shown in Figs. 1(c)–(e). Figure 1(c) reveals the presence of an imaginary frequency around the Γ point in the LDA calculations, implying that the crystal structure is unstable, whereas the phonon spectra suggest the stability of the crystal structure optimized by the GGA potential [see Figs. 1(d) and (e)]. In addition, the optimized lattice constant value of 4.861 Å is also in good agreement with experiments [12, 13]. Thus, we conclude that the GGA potential is more suitable for simulating the lattice structure of C_3N than the LDA potential, and we will discuss the electronic band structure calculated using the PBE potential throughout the rest of this paper.

In Fig. 2, we plot the electronic band structure, including the energy band dispersion, and the density of states (DOS), as well as the orbital resolved energy band structure. The figure shows an indirect band structure for C_3N with an energy gap of 0.38 eV, which is consistent with experimental observation [13]. This band structure can be easily understood in terms of the ligand field theory: One electron from a nitrogen atom in-

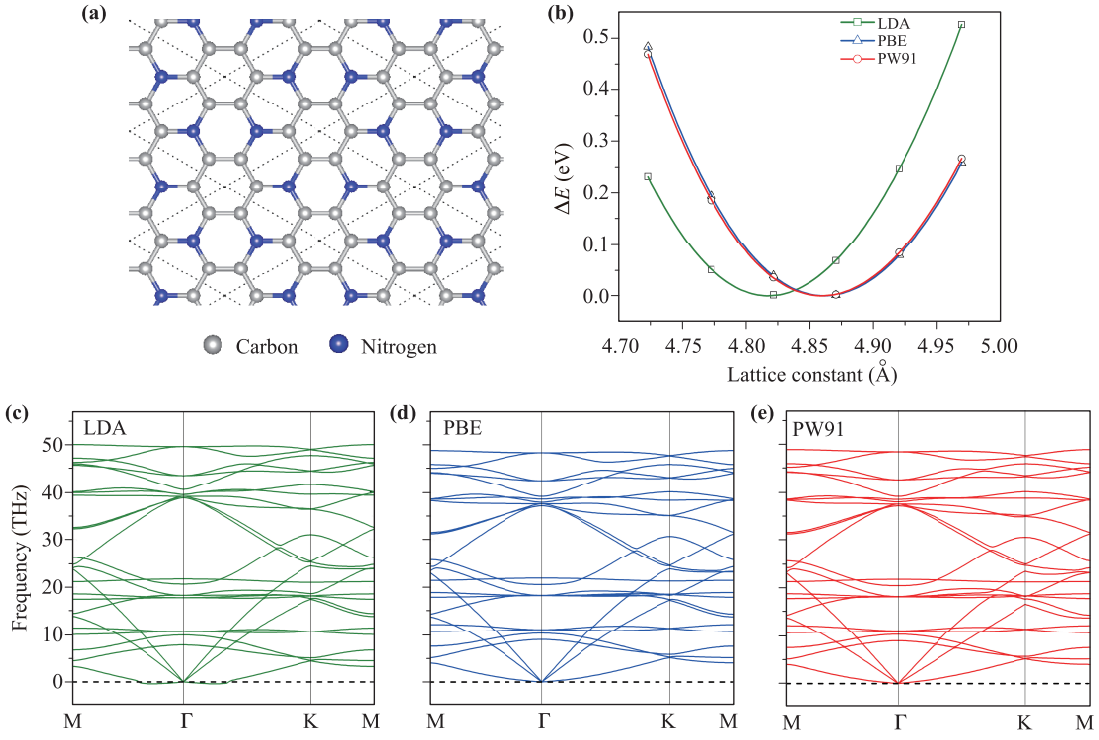

Fig. 1 **(a)** Schematic of crystal structure of C_3N. **(b)** Total energy difference ΔE as a function of the lattice constant for the LDA, PBE, and PW91 exchange-correlated potentials. **(c–e)** Corresponding phonon spectra of C_3N for the equilibrium lattice constants obtained in (b).

teracts with electrons on the three nearest-neighbor carbon atoms, forming stable chemical covalent bonds and making C_3N a semiconductor. Furthermore, it is interesting that the von Hove singularities are located near the Fermi level of ±1 eV. This feature is quite similar to that in graphene, but the energy value in C_3N is one-half that in graphene [22]. This is because the Bragg scattering at the boundary of the Brillouin zone is folded and is enhanced at one-half the energy scale when the ordered nitrogen-doped graphene forms a 2×2 superstructure. According to the well-known Stoner criterion [14, 23], if electrons are introduced into the system as charge carriers, the Fermi level moves up into the conduction band; consequently, the approach of the Fermi level to the singularity point may be associated with the ferromagnetic long-range ordered state.

To quantitatively study the effects of charge-carrier doping on C_3N, we performed electron susceptibility calculations, which provide a signature of the magnetic instability at the momentum $\boldsymbol{q}$. By applying the tight-binding model, which is fitted to the electronic band structure shown in Fig. 2(a) using the maximally localized Wannier functions [21, 24, 25], the bare electron susceptibility $\chi_0(\boldsymbol{q})$ is evaluated as [26, 27]

$$\chi_0(\boldsymbol{q}) = \sum_{\mu\nu\boldsymbol{k}} \frac{1}{N_{\boldsymbol{k}}} \frac{|\langle \boldsymbol{k}+\boldsymbol{q}, \mu | \boldsymbol{k}, \nu \rangle|^2}{E_{\mu,\boldsymbol{k}+\boldsymbol{q}} - E_{\nu,\boldsymbol{k}} + \mathrm{i}0^+} [f(E_{\nu,\boldsymbol{k}}) - f(E_{\mu,\boldsymbol{k}+\boldsymbol{q}})],$$

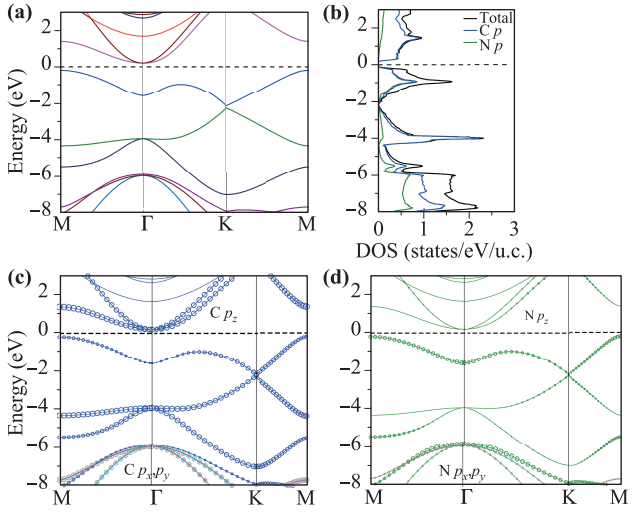

Fig. 2 **(a)** Electronic band structure of C_3N along high-symmetry $\boldsymbol{k}$ points. **(b)** Total DOS and projected DOS on C and N atoms per unit cell of C_3N. **(c, d)** Orbital resolved energy band structure of C and N atoms, respectively. The Fermi energy is set to zero.

where $E_{\mu,\boldsymbol{k}}$ represents the band energy measured at the Fermi level E_F, and $f(E_{\mu,\boldsymbol{k}})$ is the Fermi–Dirac distribution function for an eigenstate, $|\boldsymbol{k}, \mu\rangle$. In addition, $N_{\boldsymbol{k}}$ denotes the number of $\boldsymbol{k}$ points used for the irre-

ducible Brillouin zone integration. The calculated real part of the momentum-dependent electron susceptibility $\chi_0(\boldsymbol{q})$ for electron- and hole-doped C_3N is shown in Fig. 3, where we set the Fermi level to $E_F = 1.3$ eV and $E_F = -1.0$ to represent the electron and hole doping levels, respectively, on the basis of the rigid band approximation. The calculations reveal sharp peaks around the Γ point, $\boldsymbol{q} = 0$, indicating the presence of strong spin fluctuation of the ferromagnetism. This type of magnetic behavior is typically ascribed to the itinerant electron mechanism [14]. Thus, as the DOS at the Fermi level becomes larger, the spin fluctuation of the ferromagnetism becomes stronger, resulting in a higher ferromagnetic transition temperature (Curie temperature, T_c), which is also consistent with the above discussion of the Stoner criterion.

Finally, we further calculate the effect of hydrogen atoms adsorbed into C_3N as doped electron carriers in the system to check whether the system favors ferromagnetism. First, we study the system $C_3NH_{0.125}$ in the paramagnetic state, which means that no spin polarization is allowed in the calculations. This study could provide a reference for studying the magnetic states, and by analyzing the DOS at the Fermi level, we can infer whether the magnetically ordered state is favored. The DOS calculation for a nonmagnetic state in $C_3NH_{0.125}$ is shown in Fig. 4(a). A comparison with the DOS of pristine C_3N in Fig. 2(b) shows that the Fermi level moves into the conduction band, as expected from our intuition that electrons are introduced into the system via hydrogen absorption onto C_3N. However, we also notice that the features of the DOS around the Fermi level differ slightly from those of the DOS in pristine C_3N. The reason is that the local electron cloud of hydrogen atoms interacts with the electron conduction band, slightly modifying the DOS around the Fermi level. We speculate that once the Fermi level approaches the von Hove singularity, the nonmagnetic state is unstable against ferromagnetism according to the Stoner criterion. Thus, we further calculate the ferromagnetic state of $C_3NH_{0.125}$ and find that the total energy of the ferromagnetic state is lower by 3.5 meV per unit cell than that of the nonmagnetic state, suggesting that the ferromagnetic state is the ground state of $C_3NH_{0.125}$. The DOS of the ferromagnetic state is also shown in Fig. 4(b). By integrating the difference between the DOS for the spin-up and spin-down components, we evaluate the magnetic moment as $0.1\mu_B$ per unit cell, which are all in good agreement with experiments [13]. Furthermore, the projected DOS on specific atoms indicates that the ferromagnetism arises mainly from the contribution of electrons in C $2p$ orbitals, and not from the local H $1s$ orbital electrons. This result suggests that the mechanism by which ferromagnetism emerges in $C_3NH_{0.125}$ is described by the itinerant electron theory rather than the effects of local impurity coupling, which is consistent with the calculation of the electron susceptibility $\chi_0(\boldsymbol{q})$.

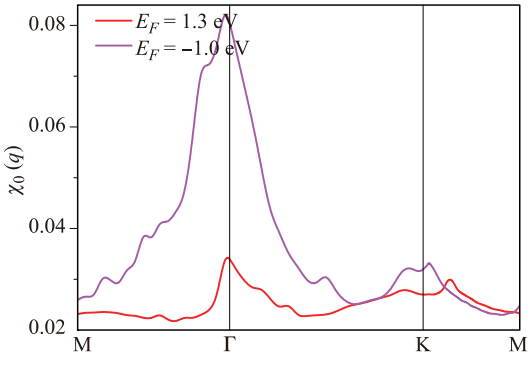

Fig. 3 Real part of bare electron susceptibility $\chi_0(\boldsymbol{q})$ along the path between high-symmetry momentum points for electron- and hole-doped C_3N, which correspond to Fermi levels of $E_F = 1.3$ eV and $E_F = -1.0$ eV, respectively.

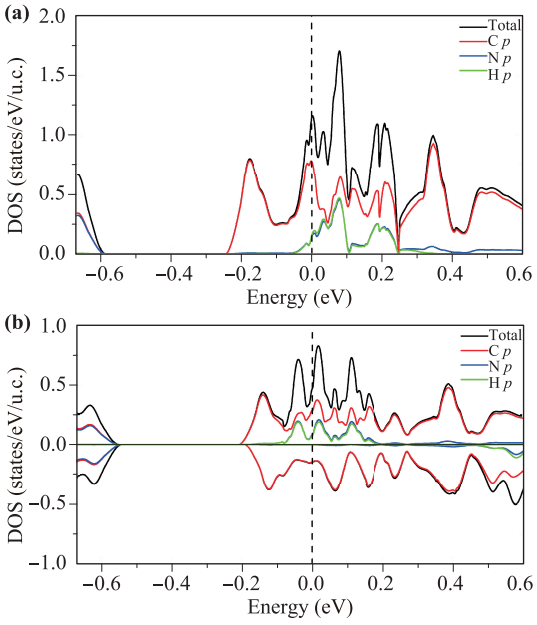

Fig. 4 Total DOS and projected DOS on carbon, nitrogen, and hydrogen atoms per unit cell of $C_3NH_{0.125}$ for the nonmagnetic state **(a)** and the ferromagnetic state **(b)**. The Fermi energy is set to zero.

4 Conclusion

We calculated the electronic and magnetic structures of the newly discovered two-dimensional quantum material C_3N using density functional (perturbation) theory and found that the C_3N system is an indirect-band semiconductor with an energy gap of 0.38 eV. More importantly,

we noticed that the intriguing von Hove singularities are located at energies near the Fermi level, ±1 eV, which is half that of graphene. When the Fermi level approaches these singularity points via charge carrier doping, the system will favor long-range magnetic order. This scenario is not only consistent with the calculation of the electron susceptibility, which has a sharp peak around the Γ point, but also in good agreement with experimental observation. In addition, calculations show that the hydrogen-doped system $C_3NH_{0.125}$ is ferromagnetic, which further confirms our conclusion. These calculations demonstrate that the emergence of magnetism is due mainly to itinerant electrons rather than the local impurity coupling mechanism, and they open an avenue to designing a field-effect transistor device for potential application of a possible insulator-ferromagnet transition realized by tuning an external electric field.

Acknowledgements We thank S. Qiao, Z. H. Kang, and Y. Lifshitz for helpful discussions. This work was supported by the Strategic Priority Research Program (B) of the Chinese Academy of Sciences (Grant No. XDB04040300), the National Natural Science Foundation of China (Grant Nos. 11404359, 21473235, 11227902, and U1632269), the Youth Innovation Promotion Association (Grant No. 2016215), and the One Hundred Person Project of the Chinese Academy of Sciences.

Appendix A Supplemental material

A.1 The lattice constant of C_3N optimized by using various exchange correlation potential

The equilibrium lattice constants are determinate by fitted from the Birch–Murnaghan isothermal equation to the total energy calculation within the framework of density functional theory via various exchange correlation pseudopotential. The Birch–Murnaghan isothermal equation of state is given by

$$E(a) = E_0 + \frac{9V_0B_0}{16}\left\{\left[\left(\frac{a_0}{a}\right)^{\frac{4}{3}} - 1\right]^3 B_0' + \left[\left(\frac{a_0}{a}\right)^{\frac{4}{3}} - 1\right]^2\left[6 - 4\left(\frac{a_0}{a}\right)^{\frac{4}{3}}\right]\right\}, \quad \text{(A1)}$$

where E is the deformed total energy, E_0 is the equilibrium total energy, a is the deformed lattice constant, a_0 is the equilibrium lattice constant, B_0 is the bulk modulus at zero pressure, B_0' is the derivative of the bulk modulus with respect to pressure, and $V_0 = 15\sqrt{3}a_0^2/2$. We treat the E_0, a_0, B_0, and B_0' as fitting parameters, which are summarized in the Table A1 for the exchange correlation potential of LDA, PBE, PW91.

Table A1 The fitting parameters of the Birch–Murnaghan isothermal equation of state for the exchange correlation potential of LDA, PBE, PW91.

Exchange correlation potential	E_0 (eV)	a_0 (Å)	B_0 (eV/Å^3)	B_0'
LDA	−77.6937	4.8174	0.9499	4.3840
PBE	−70.3077	4.8613	0.9025	4.4263
PW91	−70.4481	4.8594	0.9010	4.4313

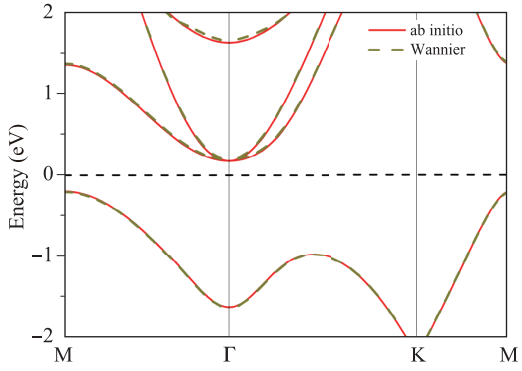

Fig. A1 Band structure of C_3N. Red solid lines represent the original band structure calculated by ab-initio calculation, and green dash lines represent Wannier fitted band structure. The Fermi energies are all set to zero.

A.2 Band structure of C_3N from an ab-initio calculation and a Wannier fitting

Using maximally localized Wannier functions within the Wannier90 code, the electronic band structure from an ab-initio calculation shown in Fig. 2(a) in the main text is well fitted, and shown in Fig. A1, which is used for the electron susceptibility calculation.

References and notes

1. K. Klitzing, G. Dorda, and M. Pepper, New method for high-accuracy determination of the fine-structure constant based on quantized Hall resistance, *Phys. Rev. Lett.* 45(6), 494 (1980)
2. D. C. Tsui, H. L. Stormer, and A. C. Gossard, Two-dimensional magneto transport in the extreme quantum limit, *Phys. Rev. Lett.* 48(22), 1559 (1982)
3. K. S. Novoselov, A. K. Geim, S. V. Morozov, D. Jiang, Y. Zhang, S. V. Dubonos, I. V. Grigorieva, and A. A. Firsov, Electric field effect in atomically thin carbon films, *Science* 306(5696), 666 (2004)
4. G. Eda, H. Yamaguchi, D. Voiry, T. Fujita, M. Chen, and M. Chhowalla, Photoluminescence from chemically exfoliated MoS_2, *Nano Lett.* 11(12), 5111 (2011)

5. J. Qiao, X. Kong, Z. X. Hu, F. Yang, and W. Ji, High mobility transport anisotropy and linear dichroism in few-layer black phosphorus, *Nat. Commun.* 5, 4475 (2014)
6. F. F. Zhu, W. J. Chen, Y. Xu, C. L. Gao, D. D. Guan, C. H. Liu, D. Qian, S. C. Zhang, and J. F. Jia, Epitaxial growth of two-dimensional stanene, *Nat. Mater.* 14(10), 1020 (2015)
7. K. Kim, J. Y. Choi, T. Kim, S. H. Cho, and H. J. Chung, A role for graphene in silicon-based semiconductor devices, *Nature* 479(7373), 338 (2011)
8. F. Schwierz, Graphene transistors, *Nat. Nanotechnol.* 5(7), 487 (2010)
9. I. Meric, M. Y. Han, A. F. Young, B. Ozyilmaz, P. Kim, and K. L. Shepard, Current saturation in zero-bandgap, topgated graphene field-effect transistors, *Nat. Nanotechnol.* 3(11), 654 (2008)
10. Y. Feng, X. Yao, M. Wang, Z. Hu, X. Luo, H. T. Wang, and L. Zhang, The atomic structures of carbon nitride sheets for cathode oxygen reduction catalysis, *J. Chem. Phys.* 138(16), 164706 (2013)
11. H. J. Xiang, B. Huang, Z. Y. Li, S. H. Wei, J. L. Yang, and X. G. Gong, Ordered semiconducting nitrogen-graphene alloys, *Phys. Rev. X* 2(1), 011003 (2012)
12. J. Mahmooda, E. K. Leea, M. Jungc, D. Shind, H. J. Choia, J. M. Seoa, S. M. Junga, D. Kimd, F. Lia, M. S. Lahd, N. Parkd, H. J. Shinc, J. H. Ohb, and J. B. Baek, Two-dimensional polyaniline (C_3N) from carbonized organic single crystals in solid state, *Proc. Natl. Acad. Sci. USA* 113, 7417 (2016)
13. S. Yang, W. Li, C. Ye, G. Wang, H. Tian, C. Zhu, P. He, G. Ding, X. Xie, Y. Liu, Y. Lifshitz, S. T. Lee, Z. Kang, and M. Jiang, C_3N-A_2D crystalline, hole-free, tunable-narrow-bandgap semiconductor with ferromagnetic properties, *Adv. Mater.* 29(16), 1605625 (2017)
14. P. Fazekas, Lecture Notes on Electron Correlation and Magnetism, World Scientific, 1999
15. M. A. Ruderman and C. Kittel, Indirect exchange coupling of nuclear magnetic moments by conduction electrons, *Phys. Rev.* 96(1), 99 (1954)
16. G. Kresse and J. Furthmuller, Efficient iterative schemes for ab initio total-energy calculations using a plane-wave basis set, *Phys. Rev. B* 54(16), 11169 (1996)
17. A. Togo and I. Tanaka, First principles phonon calculations in materials science, *Scr. Mater.* 108, 1 (2015)
18. J. P. Perdew and Y. Wang, Accurate and simple analytic representation of the electron-gas correlation energy, *Phys. Rev. B* 45(23), 13244 (1992)
19. J. P. Perdew, K. Burke, and M. Ernzerhof, Generalized gradient approximation made simple, *Phys. Rev. Lett.* 77(18), 3865 (1996)
20. F. Birch, Finite elastic strain of cubic crystals, *Phys. Rev.* 71(11), 809 (1947)
21. See Supplemental Material in detail.
22. A. H. Castro Neto, F. Guinea, N. M. R. Peres, K. S. Novoselov, and A. K. Geim, The electronic properties of graphene, *Rev. Mod. Phys.* 81(1), 109 (2009)
23. W. Li, J. X. Zhu, Y. Chen, and C. S. Ting, First-principles calculations of the electronic structure of iron-pnictide $EuFe_2(As, P)_2$ superconductors: Evidence for antiferromagnetic spin order, *Phys. Rev. B* 86(15), 155119 (2012)
24. N. Marzari and D. Vanderbilt, Maximally localized generalized Wannier functions for composite energy bands, *Phys. Rev. B* 56(20), 12847 (1997)
25. A. A. Mostofi, J. R. Yates, Y. S. Lee, I. Souza, D. Vanderbilt, and N. Marzari, Wannier90: A tool for obtaining maximally-localised Wannier functions, *Comput. Phys. Commun.* 178(9), 685 (2008)
26. X. G. Xu and W. Li, Electronic and magnetic structures of ternary iron telluride KFe_2Te_2, *Front. Phys.* 10(4), 107403 (2015)
27. K. Hu, B. Gao, Q. Ji, Y. Ma, W. Li, X. Xu, H. Zhang, G. Mu, F. Huang, C. Cai, X. Xie, and M. Jiang, Effects of electron correlation, electron-phonon coupling, and spin-orbit coupling on the isovalent Pd-substituted superconductor $SrPt_3P$, *Phys. Rev. B* 93(21), 214510 (2016)